NUCLEIC ACID THERAPEUTICS
Volume 00, Number 00, 2016

DOI: 10.1089/nat.2016.0624

Brief Communication

Anti-HIV Activities of Intramolecular G4 and Non-G4 Oligonucleotides

Maria Prokofjeva,[1,*] Vladimir Tsvetkov,[2,3,*] Dmitry Basmanov,[2] Anna Varizhuk,[1,2] Maria Lagarkova,[2] Igor Smirnov,[2] Kirill Prusakov,[2] Dmitry Klinov,[2,4] Vladimir Prassolov,[1] Galina Pozmogova,[2] and Sergey N. Mikhailov[1]

New natural and chemically modified DNA aptamers that inhibit HIV-1 activity at submicromolar concentrations (presumably via preventing viral entry into target cells) are reported. The new DNA aptamers were developed based on known intramolecular G-quadruplexes (G4s) that were functionally unrelated to HIV inhibition [the thrombin-binding aptamer and the fragment of the human oncogene promoter (*Bcl2*)]. The majority of previously described DNA inhibitors of HIV infection adopt intermolecular structures, and thus their folding variability represents an obvious disadvantage. Intramolecular architectures refold correctly after denaturation and are generally easier to handle. However, whether the G4 topology or other factors account for the anti-HIV activity of our aptamers is unknown. The impact of chemical modification (thiophosphoryl internucleotide linkages) on aptamer activity is discussed. The exact secondary structures of the active compounds and further elucidation of their mechanisms of action hopefully will be the subjects of future studies.

Keywords: HIV, inhibition, aptamer, phosphorothioate, lentivirus

Introduction

G-QUADRUPLEX (G4) APTAMERS have recently emerged as potentially promising therapeutic agents and attractive tools for targeted drug delivery, molecular imaging, and biosensor construction [1,2]. Rational aptamer design based on known active G4 scaffolds initially selected from combinatorial oligonucleotide (ON) libraries through SELEX (systematic evolution of ligands by exponential enrichment) and post-SELEX chemical modifications are reasonable strategies to obtain potent antiviral ONs, especially HIV inhibitors [3,4]. To date, the following G4 aptamer families targeting different HIV-1 proteins have been reported:

(1) aptamers to reverse transcriptase (RT) (eg, the intramolecular antiparallel G4-forming ON d(GGGGG TGGGAGGGTAGGCCTTAGGTTTCTGA) [5]);
(2) aptamers to the envelope glycoproteins gp120 and/or gp41 (eg, the tetramolecular parallel G4-forming thiophosphoryl ON d(TTGGGTT) [6] and terminally modified hexamer d(TGGGAG) [7,8]);
(3) aptamers to the HIV integrase (IN) (eg, the ON d(GG GGTGGGAGGAGGGT) known as 93del, which adopts a dimeric ''interlocked'' parallel G4 structure with an AG4 pentad sandwiched between G-tetrads [9]; the thiophosphoryl ON d(GGGTTTTGGG), which folds into a dimeric antiparallel G4 [10]; the intramolecular antiparallel G4-forming ON Zintevir (also known as AR177 and T30177) d(G*TGGTGG GTGGGTGGG*T), where * is a thiophosphoryl internucleotide linkage [11]; and the Zintevir analogs d(GTGGTGGGTGGGTGGGT) (T30175), d(G*GGT GGGTGGGTGGG*T) (T30695), and d(GGGT)4 (T30923) [11–13] with ambiguous folding [14,15]).

Notably, some of these aptamers can act as multimodal HIV inhibitors. The ''interlocked'' aptamer 93del was initially selected against the RNase H domain of HIV-1 RT but exhibited anti-IN activity *in vitro* [16] and interfered with viral entry, reverse transcription, and integration in cells [17]. Similarly, Zintevir and its derivatives were initially selected against HIV-1 IN, but subsequent studies revealed that gp120 might be their primary target [18]. Aptamer binding to gp120 generally interferes with interactions between gp120 and the cellular receptors (CD4 and co-receptors), thereby preventing viral attachment.

[1]Engelhardt Institute of Molecular Biology RAS, Moscow, Russia.
[2]Federal Research and Clinical Center of Physical-Chemical Medicine of Federal Medical Biological Agency, Moscow, Russia.
[3]Topchiev Institute of Petrochemical Synthesis Russian Academy of Sciences, Moscow, Russia.
[4]Moscow Institute of Physics and Technology (State University), Moscow Region, Russia.
*These two authors contributed equally to this work.

Structure-activity and stability-activity relationships have been investigated to some extent for several G4 HIV inhibitors [19]. The most rigorously studied aptamers are probably the 5′-substituted Hotoda's ONs d(TGGGAG) [7,8], which target HIV-1 entry through gp120 binding [20]. These hexamers adopt a tetramolecular parallel G4 topology with four G-tetrads and one internal A-tetrad [21]. 5′-Terminal hydrophobic moieties (dimethoxytrityl, DMTr [22], 3,4-dibenzyloxybenzyl [20], tert-butyldiphenylsilyl [23] or other aromatic groups [24]) significantly contribute to aptamer activity, presumably by direct participation in aptamer-protein interactions [25]. It has been also been assumed that the modifications facilitate G4-folding, but recent findings argue against this assumption [26].

Other modifications that enhance aptamer activity include the introduction of a 2-hydroxy-ethylphosphate group at the 3′-terminus [7,8] and conjugation with monosaccharide (glucose or mannose) residues [27]. Substitutions of the core guanines for conformationally constrained ''locked'' nucleic acid monomers at certain positions resulted in potent aptamers with increased thermal stability [28]. However, the correlation between G4 stability and overall aptamer activity is not strict. Bulky pyrene derivatives at the 5′-terminus alter G4-folding and lead to activity loss [28], which argues for the importance of parallel G4-folding for efficient target recognition.

To summarize, the analysis of active G4-DNA HIV inhibitors reveals the following tendencies:

- The most common scaffolds are the antiparallel G4 core and the four-tetrad parallel G4 core.
- G-T-rich sequences are abundant, which is hardly surprising because thymine in loops is thermodynamically more favorable than adenine (its exposure to solution results in lower solvation entropy), whereas C-rich fragments (if present) induce the formation of Watson-Crick hairpins. Interestingly, adenines in G4-forming sequences may also be beneficial (eg, participate in the formation of noncanonical tetrads or pentads).
- Terminal chemical modifications (especially hydrophobic modifications) can increase G4 thermal stability, whereas local backbone modifications, such as thiophosphoryl internucleotide fragments, are typically used to endow aptamers with resistance to nucleases and to enhance aptamer-binding affinity [29].

Many potent inhibitors of HIV-1 entry (eg, d(TTGGGTT) [6], Hotoda's aptamer and its derivatives) form intermolecular structures. The intermolecular G4 arrangement is generally prone to conformational polymorphisms and concentration-dependant rearrangements, which complicates handling of these aptamers and poses limitations on their practical application. Several attempts have been made to overcome this problem in Hotoda's hexanucleotides. Piccialli and colleagues employed the TEL-ODN strategy (tetra-end-linked oligodeoxynucleotides) [30,31] (ie, they joined the 3′-termini of the four 5′-end-substituted hexanucleotides through a tetra-branched linker to obtain active pseudointrameric G4s). Although this strategy has proven to be rather efficient, the preparation of TEL-G4 requires significant synthetic effort and we have chosen a different approach here. We designed a series of native and chemically modified ONs using intramolecular G4s as basic scaffolds and tested their anti-HIV activities.

The abovementioned multimodal function of several HIV inhibitors and the diverse cross-reactivity of genomic G4s prompted us to search for appropriate G4 scaffolds among already known but seemingly unrelated intramolecular aptamers. SELEX, which is the gold standard methodology for the development of specific aptamers, is often time-consuming and suffers from a relatively low success rate [32]. We hypothesized that exploiting the potential of the existing aptamer pool might be as productive as *de novo* selection if preliminary knowledge about the structure-activity relationship was available.

The thrombin-binding aptamer (TBA) [33] has been comprehensively characterized and is arguably one of the most celebrated G4 structures. TBA forms an antiparallel chair-type 2-tetrad G4 with $T_m = 52°C \pm 1°C$ in the presence of 100 mM KCl [34]. The GT-richness and the antiparallel folding of this aptamer suggested that it could possess some antiviral activity (see the general features of known active G4-DNA HIV inhibitors). TBA has not been considered as an antiviral agent to date but has been shown to interact with the HIV nucleocapsid protein [35].

TBA has also demonstrated significant antiproliferative activity in human cell cultures [36]. Until recently, there had been no follow-up on the latter finding because the anticoagulant properties of TBA hampered its potential anticancer applications. Eventually, a suitable chemical modification that preserved the antiproliferative activity of TBA over its anticoagulant actions was reported [37]. This finding is likely to reinvigorate interest in TBA analogs with respect to cancer treatment and illustrates the multifunctional potential of aptamer scaffolds.

In the context of the transmission of viral infection, blood clotting inhibition may be a double-edged sword. For catheter-related bloodstream infections, the dual antiviral-anticoagulant action of the aptamer may be an advantage because it will simultaneously solve the problem of catheter blockage [38]. However, in cases of vaginal transmission, anticoagulants might exacerbate the effects of ulceration. Some polyanionic microbicides that have entered clinical trials have demonstrated anticoagulant activities [39,40]; therefore, the risk of ulceration is a common problem.

Materials and Methods

ON synthesis, purification, and MS analysis

ONs were synthesized on a Biosset ASM-800 DNA synthesizer following standard phosphoramidite protocols and purified by preparative scale reverse phase high-performance liquid chromatography (HPLC) on a 250 mm × 4.0 mm Hypersil C18 column with detection at 260 nm and a 12%–24% gradient of CH_3CN in 0.1 M ammonium acetate buffer. The DMTr protection group was removed via treatment with 80% acetic acid for 20 min (this step was skipped for DMT-thio-BclON). The detritylated ONs were further purified in a 0%–12% CH_3CN gradient in 0.1 M ammonium acetate buffer. The purity of all ONs was determined to be 95% by HPLC. The matrix-assisted laser desorption/ionization time-of-flight (MALDI-TOF) mass spectra of the ONs were acquired on a Bruker Microflex mass spectrometer in linear mode (20 kV). Each spectrum was accumulated using 200 laser shots (N_2 gas laser, 337 nm). A solution of 35 g/mL of 3-hydroxypicolinic acid with dibasic ammonium citrate was used as the matrix.

Circular dichroism, ultraviolet-melting and fluorescence resonance energy transfer experiments

ONs were dissolved in a 20 mM Tris-HCl buffer (pH 7.5) containing 10 mM KCl, 100 mM KCl or 100 mM LiCl, denatured at 95°C for 5 min and snap cooled on ice before all measurements to ensure intramolecular folding. The ultraviolet (UV) spectra, circular dichroism (CD) spectra and UV melting curves were recorded on a Chirascan spectrophotometer (Applied Photophysics) equipped with a thermostated cuvette holder. The melting temperatures of the quadruplexes were estimated from the maximum in the first derivative of the melting curve. The absorbance was registered every 1°C across the 20°C–90°C temperature range (heating rate = 0.5°C/min). The rotational relaxation times (RRTs) of ethidium bromide (EtBr) bound to the ONs were determined as described in Ref. [41]. In the fluorescence resonance energy transfer (FRET) experiments, the 6-carboxyfluorescein (FAM) fluorescence was measured with a Cary Eclipse Fluorescence Spectrophotometer (Agilent Technologies) at 20°C. The excitation wavelength was 480 nm. The polarization of FAM fluorescence at 520 nm was determined as described in Ref. [41].

Assessment of ON inhibitory activity

The Jurkat cell line was cultured in RPMI 1640 medium containing 20% fetal calf serum, 4 mM L-glutamine, 100 U/mL of penicillin, and 100 μg/mL of streptomycin. The cells were grown at 37°C in a humidified chamber containing 5% CO_2. A solution of the analyzed substance (ON, chitosan sulfate or dextran sulfate) in water or dimethyl sulfoxide (the final concentration in the medium was no higher than 0.1%) was added to the cells; after 1 h, the cells were transduced with pseudo-HIV-1 particles obtained as described in Refs. [42,43]. The relative level of transduction was determined by flow cytometry using an Epics 4XL Beckman Coulter instrument 48 h post-transduction.

Toxicity studies

The influence of ONs on cell proliferation was measured on suspension Jurkat cells using MTT Cell Proliferation Kit (OZ Biosciences). Cells were cultured in 96-well plates. ONs were added to culture medium at concentrations of 0, 0.1, 1, 5, 10, and 20 μg/mL for 48 h. Each concentration was evaluated in triplicate. The metabolic activity (farmazan production) was measured according to the suspension cells protocol provided by the manufacturer. The absorbance of the converted dye was measured on a plate reader at 570 nm and a reference wavelength at 650 nm. The signal was calculated as OD570–OD650, and the results were expressed as a percentage of control (nontreated) cells.

The influence of ONs on cell viability was measured on Jurkat cells by fluorescence-activated cell sorting (FACS) analysis after propidium iodide (PI) staining of unfixed cells. Cells were cultured in 96-well plates. ONs were added into culture medium at concentrations of 0, 0.1, 1, 5, 10, and 20 μg/mL for 48 h. After treatment PI staining solution was added to each sample just before FACS analysis.

Photonic crystal surface wave experiments

Streptavidin-coated 1D photonic crystal slides were prepared as described in Ref. [44]. The surface was blocked with a bovine serum albumin (BSA) solution in phosphate-buffered saline (PBS) buffer [10 mM NaH_2PO_4/Na_2HPO_4 (pH 7.4), 137 mM NaCl, and 2.7 mM KCl]. The biotinylated ON solution (50 nM) in PBS was pumped through the working chamber until signal saturation was achieved and washed with PBS. The gp120 solution (various concentrations) in PBS was subsequently injected and run over the ON-coated 1D PC surface for ~1,000 s (time required for signal saturation); then, the chamber was washed with the buffer for an additional 500 s (flow rate = 50 μL/min).

Streptavidin was purchased from Sigma-Aldrich, gp120 was purchased from Speed BioSystems, and BSA was purchased from Thermo Fisher Scientific.

Molecular modeling

Model preparation for the docking experiments. Three-dimensional models of the aptamers were obtained using the nuclear magnetic resonance -based structure of unmodified TBA in complex with human thrombin PDB 1HAO [45]. The protein was removed, and in the case of F-thio-TBA one oxygen atom of each phosphate internucleotide linkage in TBA was substituted with sulfur to produce diastereomers with all-*R*, all-*S*, or alternating *R/S* P configurations. Partial atomic charges of the thiophosphoryl linkage atoms were obtained by single-point energy quantum mechanics calculations. Electron density in thiophosphoryl linkages (including C3′ and C5′) was calculated by the *ab initio* quantum mechanical method (density functional theory [46]) with hybrid exchange-correlation functional B3LYP and the 6-31G(d) basis set. Based on the calculated electron density distribution, the partial atomic charges were computed using the Mulliken's population analysis scheme [47]. The choice of the scheme for calculating partial atomic charges is explained in [44]. All quantum mechanics simulations were carried out using the Gaussian 09 program.

The gp120 model was taken from PDB 2B4C [48] and optimized using the SYBYL 8.0 molecular graphics software package (Tripos, Inc.). Unfavorable van der Waals interactions were removed by short molecular mechanics minimizations using Powell's method [49] with the following settings: estimation of the partial atomic charge with application to Gasteiger–Hückel method [50], assignment of the atom types from TRIPOS force field [51], nonbonded cutoff distance equal to 8 Å, solvent effect accounting via the distance-dependent dielectric function, 1,000 iterations, simplex method in the initial optimization, and energy gradient convergence criterion with a threshold of 0.05 kcal mol^{-1} $Å^{-1}$.

Docking. Flexible docking of the aptamers to full-sized gp120 was performed with Autodock 4.2 [52] to define the putative binding sites. The protein and aptamers were prepared for docking using AutodockTools (ADT Version 1.5.4). The 3D grid maps ($126 \times 126 \times 126$ points with 0.375 Å spacing) for each atom type were computed using AutoGrid4. Additionally, electrostatic and desolvation maps were calculated. Because viral adsorption and fusion occur via gp120 interactions with the CD4 receptor and chemokine receptor CCR5 with active participation of the V3 loop, docking was performed at areas containing the CD4- and CCR5-binding sites in gp120 and its V3 loop.

The side chains of the amino acid residues LYS97, ASN279, LYS282, HIS363, ASN461, ARG469, ARG476,

and ARG480 were flexible upon aptamer docking to gp120 in the proximity of the CD4-binding site. The side chains of GLN301, ARG304, LYS305, ARG315, ARG327, HIS308, ARG419, GLN422, and LYS432 were flexible upon docking near the CCR5-binding site. The side chains of THR297, ARG298, ASN300, GLN301, ASN302, ARG304, LYS305, THR303, ILE307, HIS308, ARG315, ARG327, ASP325, PHE317, TYR318, HIS330, SER306, and ILE309 were flexible upon docking to the V3 loop. The G4 core was fixed in the aptamers but the nucleobases in the loops were allowed to rotate around the glycosidic bonds.

The Lamarckian genetic algorithm (GA-LS) [53], which is a hybrid of a genetic and local search algorithm, was applied to identify the most probable binding site. The following GA-LS parameters were used: 100 GA-LS runs, 2,500,000 energy maximum, maximum of 27,000 generations, and mutation and crossover rates of 2 and 0.8, respectively. The Pseudo-Solis and Wets parameters were used for the local search algorithm with the number of iterations set to 300. The starting positions and conformations of the aptamers were random. The torsion angle rotation step was 50°. After docking, all generated structures were clustered with a root-mean-square tolerance of 2 Å from the lowest energy. Free energies of aptamer binding with the gp120 sites were estimated using force field scoring functions and the formula:

$$\Delta G_{\text{binding}} = \Delta G_{\text{elec}} + \Delta G_{\text{solv}} + \Delta G_{\text{vdW}} + \Delta G_{\text{H-bond}}$$

The parameter ΔG_{elec} was calculated by the distance-dependent dielectric of Mehler and Solmajer [54]. Van der Waals interactions (ΔG_{vdW}) were estimated using the Lennard-Jones potential and atomic parameters from the AMBER force field. For scoring of the H-bond energy ($\Delta G_{\text{H-bond}}$), the 10/12 potential was used with a maximum well depth of 5 kcal/mol at 1.9 Å for hydrogen bonds with oxygen and nitrogen atoms and then multiplied by the function estimation rate from the ideal H-bonding geometry. To estimate the desolvation energy (ΔG_{desolv}), we used the atomic fragmental volume and solvation parameters derived from the method of Stouten *et al.* [55]. Each term was multiplied by semi-empirical weighting constants by fitting a training set of complexes with known structures to the binding affinity data. The scoring function in the docking procedure also involved the conformational entropy ΔG_{tors}. The change in the aptamer conformational mobility was solely estimated by calculating the number of dihedral angles.

The precise calculation of ΔG_{tors} might be difficult in our models for the following two reasons: (1) conformational changes in gp120 and the aptamers could substantially contribute to ΔG_{tors} but could not be accurately estimated and (2) the weighting constant for ΔG_{tors} might be incorrect because the regression multipliers for this parameter were obtained for chemical structures that were significantly different from the investigated aptamers. Therefore, the ΔG_{tors} values were omitted from the analysis.

Molecular dynamics simulation. The explicit (TIP3P) solvent simulations were performed using the Amber 14 suite in a cubic water box with periodic boundary conditions imposed. The parameters of all atoms needed for interatomic energy calculations were taken from the force fields ff14SB and GLYCAM_06j-1. The negative charges were neutralized by adding Na^+ ions, and ~19,000 water molecules were employed for solvation. A K^+ cation was placed in the center of the aptamer between the quartets to stabilize the structure. The structures were minimized before the simulations.

First, the locations of the solvent molecules were optimized for 1,000 steps (500 steps of a steepest descent minimization followed by 500 steps of a conjugate gradient minimization), with all the solute atoms being restrained to their positions with a force constant of 500 kcal mol^{-1} Å^{-2}. Then, the complex structure was optimized without any restriction for 2,500 steps (1,000 steps of steepest decent followed by 1,500 steps of conjugate gradient). Subsequently, a gradual heating to 300 K over 20 ps was performed. To avoid wild fluctuations in the system at this stage, weak harmonic restraints with a force constant of 10 kcal mol^{-1} Å^{-2} were used for all atoms with the exception of the solvent atoms. All bonds to hydrogen atoms were constrained using the SHAKE algorithm [56], which allowed a time step of 2 fs. The non-bound one to four van der Waals and electrostatic interactions were scaled by standard amber values (SCEE = 1.2, SCNB = 2.0). The cutoff for van der Waals interactions was set to 10 Å. Long-range electrostatics was calculated using the particle mesh Ewald method.

The molecular dynamics (MD) simulations in a production phase were performed at $p = 1$ atm and $T = 300$ K under the control of a Langevin thermostat with a collision frequency of 1 ps^{-1}. The trajectory length was 8 ns. Snapshot visualization was performed using VMD software (www.ks.uiuc.edu/Research/vmd). The molecular mechanics with the generalized Born and surface area solvation (MM-GBSA) analysis was performed as described in Ref. [44]. Ensemble averages and standard deviations of the free energy and its components were calculated by means of Gibbs–Boltzmann distribution for the ensemble of conformations obtained from the trajectory computed during the production phase.

Results and Discussion

ON design and secondary structure analysis

As has been mentioned in the Introduction section, TBA could be considered as a scaffold for developing anti-HIV candidates because of its relative structural resemblance to known HIV inhibitors, but the anticoagulant activity has to be minimized (eg, via chemical modification). Previously, we analyzed TBA analogs with thiophosphoryl internucleotide linkages [34,44,57]. The thio-modification was shown to reduce anticoagulant activity [57] and had various effects on the thermal stability of the aptamer (from moderate destabilization to slight stabilization) depending on the position and number of thio-linkages [34]. The modification is also known to increase toxicity (a major disadvantage) and improve ON resistance to nuclease cleavage [58]. We assumed that TBA analogs with high thermal and enzymatic stability but reduced anticoagulant activity might merit testing as microbicide candidates.

The sequences of all ONs tested are provided in Table 1. Thio-TBA is a TBA derivative with thiophosphoryl internucleotide linkages in the TT loops. It is a slightly less potent thrombin inhibitor than TBA but has slightly enhanced thermal stability ($T_m = 54°C \pm 1°C$ in the presence of 100 mM KCl) and substantially enhanced resistance to nuclease

Table 1. G4 ONs and Their Derivatives: Structural Characteristics and Anti-HIV Activities

ON code	*Sequence, 5′-3′*	*m/z, found (calc. for $[M+H]^+$)*	*G4 type*	*IC_{50}, μg/mL*	*IC_{50}, nM*
TBA	d(GGTTGGTGTGGTTGG)	4727 (4727)	Anti	>10	>2,000
Thio-TBA	d($GG_{thio}T_{thio}T_{thio}GGTGTGG_{thio}T_{thio}T_{thio}GG$)	4822 (4822)	Anti	1.6 ± 0.4	320 ± 80
F-thio-TBA	Thio-d(GGTTGGTGTGGTTGG)	4952 (4951)	Anti	0.179 ± 0.008	36 ± 2
BclON	GGGGGCCGTGGGGTGGGAGCTGGGG	7956 (7958)	Hybrid	0.46 ± 0.02	58 ± 3
BclON-mut	GGGGGCCGTTTTTTGGGAGCTGGGG	7857 (7858)	Hybrid or no G4	0.08 ± 0.03	10 ± 4
F-thio-BclON	Thio-d(GGGGGCCGTGGGGTGGG AGCTGGGG)	8341 (8342)	Hybrid	0.040 ± 0.003	4.8 ± 0.4
DMT-thio-BclON	DMTr-Thio-d(GGGGGCCGTGGGGTGG GAGCTGGGG)	8341 (8342)[a]	n/a	0.018 ± 0.002	2.1 ± 0.2
N25	d(NNNNNNNNNNNNNNNNNNNNNNNN)	7168–8186	n/a	—	—

[a]The DMT group is cleaved under the conditions of MALDI-TOF MS.

IC_{50} values of control non-ON HIV-1 inhibitors chitosan sulfate and dextran sulfate were 0.06 ± 0.03 and 0.11 ± 0.04 μg/mL, respectively. N25 is a mixture of random sequence 25-mers obtained by solid-phase synthesis using an equal mixture of all four phosphoramidites at each step. Its activity inhibitory was within experimental error.

Anti, antiparallel intramolecular G4; CD, circular dichroism; hybrid, hybrid (mostly parallel) intramolecular G4 (determined by CD and RRT analysis); MALDI-TOF MS, matrix-assisted laser desorption/ionization time-of-flight mass spectrometry; n/a, not analyzed; ON, oligonucleotide; RRT, rotational relaxation time; TBA, thrombin-binding aptamer; Thio, thiophosphoryl internucleotide linkage.

digestion [57]. F-thio-TBA (the ''fully modified'' aptamer) bears thiophosphoryl internucleotide linkages throughout the chain. It is less thermostable than TBA ($T_m = 45°C \pm 1°C$ in the presence of 100 mM KCl) but exhibits no anticoagulant activity [44]. Both thio-analogs of TBA retain the antiparallel folding pattern (see Ref. [34] for CD spectra and melting curves).

The other scaffold used in this study is a fragment of the human *Bcl2* promoter region (chr18: −60985942 to −60985966, BclON) (Table 1). Direct involvement of this highly conserved G4 motif, located 42 nucleotides upstream of the translation start site, in post-translational modulation of *Bcl2* expression has been demonstrated [59]. A number of genomic G4 motifs have been previously considered as aptamer candidates [60] or ON decoys [61,62], and a promoter-derived G4 aptamer selection method (G4PAS) has been proposed [63]. Generally, genomic noncanonical structures appear to be promising aptamer scaffolds. Parallel intramolecular G4s from oncogene promoters are probably most suitable for antitumor drug design because their folding is associated with cancer-selective cell binding and antiproliferative activities [64,65]. We hypothesized that these G4s might also have potential utility as antiviral agent scaffolds because parallel G4s are rather common among known ON inhibitors of HIV (see Introduction section).

To date, the BclON secondary structure has not been reported but its RNA analog has been shown to form an intramolecular parallel G4 [59]. The CD spectra of BclON and its thiophosphoryl derivative F-thio-BclON (Supplementary Fig. S1A; Supplementary Data are available online at www.liebertpub.com/nat) bear features that are characteristic of both parallel (a positive band near 265 nm and a negative band near 245 nm) and antiparallel G4s (a positive band near 295 nm). Thus, BclON and F-thio-BclON adopt hybrid topologies. The contribution of parallel folding (stacked G-tetrads with the same polarities) is more pronounced. In the presence of 100 mM KCl, the T_m values of BclON and F-thio-BclON were close to or above 80°C; the lower plateau of the melting curve was not observed and we were unable to accurately compare thermal stabilities. Therefore, we performed melting experiments (Supplementary Fig. S1B) at a moderate (10 mM) salt concentration ($T_m^{BclON} = 58°C \pm 1°C$; $T_m^{F\text{-}thio\text{-}BclON} = 62°C \pm 1°C$).

BclON-mut is a mutant of BclON designed to form no intramolecular G4 structures. Indeed, a negative peak at 295 nm was absent in the thermal difference spectrum of this mutant (Supplementary Fig. S1C) and no UV-melting at 295 or clear CD-melting at 265 nm was observed. The CD spectrum (Supplementary Fig. S1A) resembles a parallel quadruplex but the molar ellipticity at 265 nm is low, which argues against stable G4.

Intramolecular folding of BclON and BclON-mut after rapid annealing was confirmed by analyzing the RRTs of EtBr bound to ONs, which are roughly proportional to the hydrodynamic volumes of the complexes (Supplementary Fig. S1D). To clarify whether BclON-mut can adopt dimeric or tetrameric structures at higher concentrations, additional experiments with the slowly annealed samples were performed (Supplementary Fig. S2). Apparent concentration-dependence and salt-dependence of molar ellipticity at 265 nm and relatively sharp melting curves at 50 μM BclON-mut concentration indicate the presence of intermolecular G4s. At submicromolar concentrations their contribution would be low.

A traditional definition of a G4 motif that stipulates uninterrupted G_{3+} runs suggests three-tetrad BclON/F-thio-BclON structures. The ratio of CD amplitudes at 295 and 265 nm argues for two stacked quartets with similar polarities and a third quartet with the opposite polarity [66]. However, high thermal stabilities of these G4s suggest more complex structures with additional stacking (eg, four-tetrad G4s with G-vacancies [67] and/or bulging nucleotides [68]) (Supplementary Fig. S1E). The exact secondary structures of BclON and its derivatives hopefully will be addressed in future studies.

General assessment of anti-HIV-1 activity

The inhibitory activities of the ONs were assessed using a lentiviral system [42,43]. Jurkat cells were transduced with

pseudo-HIV particles containing HIV enzymes, recombinant GFP-coding RNA, and the HIV gp160 surface proteins (gp41 and gp120). Cell transduction resulted in GFP expression. The transduction efficiency in the presence of the ON inhibitors was monitored by GFP fluorescence. The results are summarized in Fig. 1 and the IC_{50} values are given in Table 1. The IC_{50} values were calculated by fitting the experimental data (transduction efficiencies at different inhibitor concentrations) to the standard dose–response equation (Supplementary Fig. S3). Interestingly, the dose–response curves obtained for the TBA derivatives suggest Hill coefficient [Hill Slope (HS)] values very close to 1 (which argues for 1:1 binding), whereas in the case of the BclON series, HS values other than 1 were obtained (which indicates multiple ligand binding) [69].

To exclude the possibility of ON toxicity interference with transduction efficiency measurements, we evaluated ON effects on proliferation and viability of Jurkat cells using the standard MTT test and FACS analysis (Supplementary Fig. S4). No significant effects were observed at ON concentrations up to 20 μg/mL.

All ONs with the exception of TBA and thio-TBA demonstrated relatively high inhibitory activities. The BclON derivatives were generally more active than the TBA derivatives. Unmodified TBA demonstrated minimal activity (comparable to that of the random ON N25 used as a negative control), whereas unmodified BclON and BclON-mut inhibited lentiviral transduction in the nanomolar range.

The well-known intramolecular G4 inhibitor of HIV infection Zintevir ($IC_{50} = 2.4$ μg/mL according to Ref. [18]) has been reported to be less efficient than the control non-ON inhibitor dextran sulfate ($IC_{50} = 0.8$ μg/mL according to Ref. [18]). In our experiments, BclON-mut, F-thio-BclON, and DMT-thio-BclON (IC_{50} values: 0.08 ± 0.03, 0.040 ± 0.003, and 0.018 ± 0.002 μg/mL, respectively) were superior to dextran sulfate ($IC_{50} = 0.11 \pm 0.04$ μg/mL, Fig. 1). Although direct comparison of our data with the data in the literature would be inappropriate because different methods, conditions, and cell lines were used, it is apparent that F-thio-BclON and DMT-thio-BclON are highly potent inhibitors of lentiviral transduction that should be tested against wild-type HIV and can be considered as microbicide candidates. Although BclON and BclON-mut are less active, they may be even more promising because lower (if any) general toxicity can be expected for these natural ONs relative to the thiophosphoryl ONs.

ON binding with the HIV gp120 glycoprotein

Many known G4 inhibitors of HIV-1, including aptamers with multimode action, have been reported to prevent viral entry and have demonstrated affinities toward the viral glycoproteins [6,18,23]. The HIV envelope glycoprotein consists of an exterior domain (gp120) and a transmembrane domain (gp41). Interactions with a cellular CD4 receptor (the attachment step of viral entry) trigger conformational rearrangements in gp120 that allow it to engage a co-receptor (ie, the chemokine receptor CCR5 or CXCR4). Co-receptor binding exposes a hydrophobic region (fusion peptide) in gp41and leads to the fusion of the viral envelope with the cellular membrane [70].

Our lentiviral transduction experiments were performed in the absence of transfectants. Therefore, we assumed that the observed inhibitory activities of BclON and the TBA derivatives could be at least partially attributed to their interference with pseudo-viral entry. Additionally, an ON interaction with intracellular targets cannot be excluded because ONs (especially thiophosphoryl ONs) can theoretically enter cells at pharmacologically relevant concentrations even without transfection reagents [71].

To verify the hypothesis of viral attachment inhibition, we studied interactions of the leading unmodified ONs BclON and BclON-mut with recombinant gp120 using a photonic crystal surface wave biosensor (http://pcbiosensors.com) with independent registration of the angle of total internal reflection from the liquid [72]. The first implementation of this method for an investigation of aptamer-protein binding was reported in our previous work [44]. Here, we synthesized

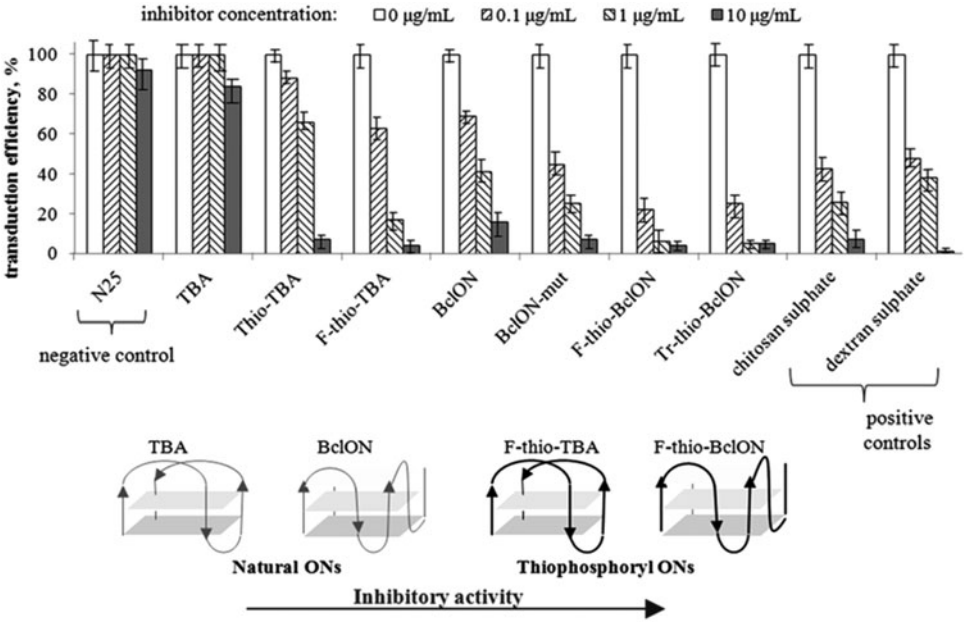

FIG. 1. Suppression of HIV-1 lentiviral transduction by G4 ONs and their derivatives. Lentiviral transduction was estimated by calculating the number of fluorescent cells transduced with pseudo-HIV particles in the presence of the ON inhibitors. Known non-ON inhibitors of viral entry (chitosan sulfate and dextran sulfate) were used as positive controls. N25 is a mixture of random-sequence 25-mer ONs that is used as the negative control. The data represent mean values of two experiments performed in duplicate. ONs, oligonucleotides.

biotinylated analogs of BclON and BclON-mut [d(GGGGG CCGTGGGGTGGGAGCTGGGGTTTTT)-biot (the T5-linker is in italics; m/z calc. $[M+H]^+$, 9884; found, 9888) and d(GGGGGCCGTTTTTTGGGAGCTGGGGTTTTT)-biot (m/z calc. $[M+H]^+$, 9784; found, 9785), respectively].

The biotinylated ONs were immobilized on the streptavidin-coated biosensor working surface and different gp120 concentrations in PBS buffer were added. The obtained sensorgrams are shown in Fig. 2A (top graphs). Equilibrium increments of the effective adlayer thickness upon gp120 binding with the immobilized ONs were used to assess the binding constants (Fig. 2A, bottom graphs). The ONs demonstrated comparable affinities toward gp120 ($K_D^{BclON} = 86 \pm 17$ nM and $K_D^{BclON\text{-}mut} = 143 \pm 79$ nM). Interestingly, the BclON/gp120 K_D value was rather close to the BclON IC_{50} value, which indirectly supports the assumption that the anti-HIV activity of BclON is primarily due to its interaction with gp120.

To clarify whether BclON retained the G4 conformation or was unwound upon binding, we chose the FRET method (Supplementary Fig. S5), which allowed us to use low ON and

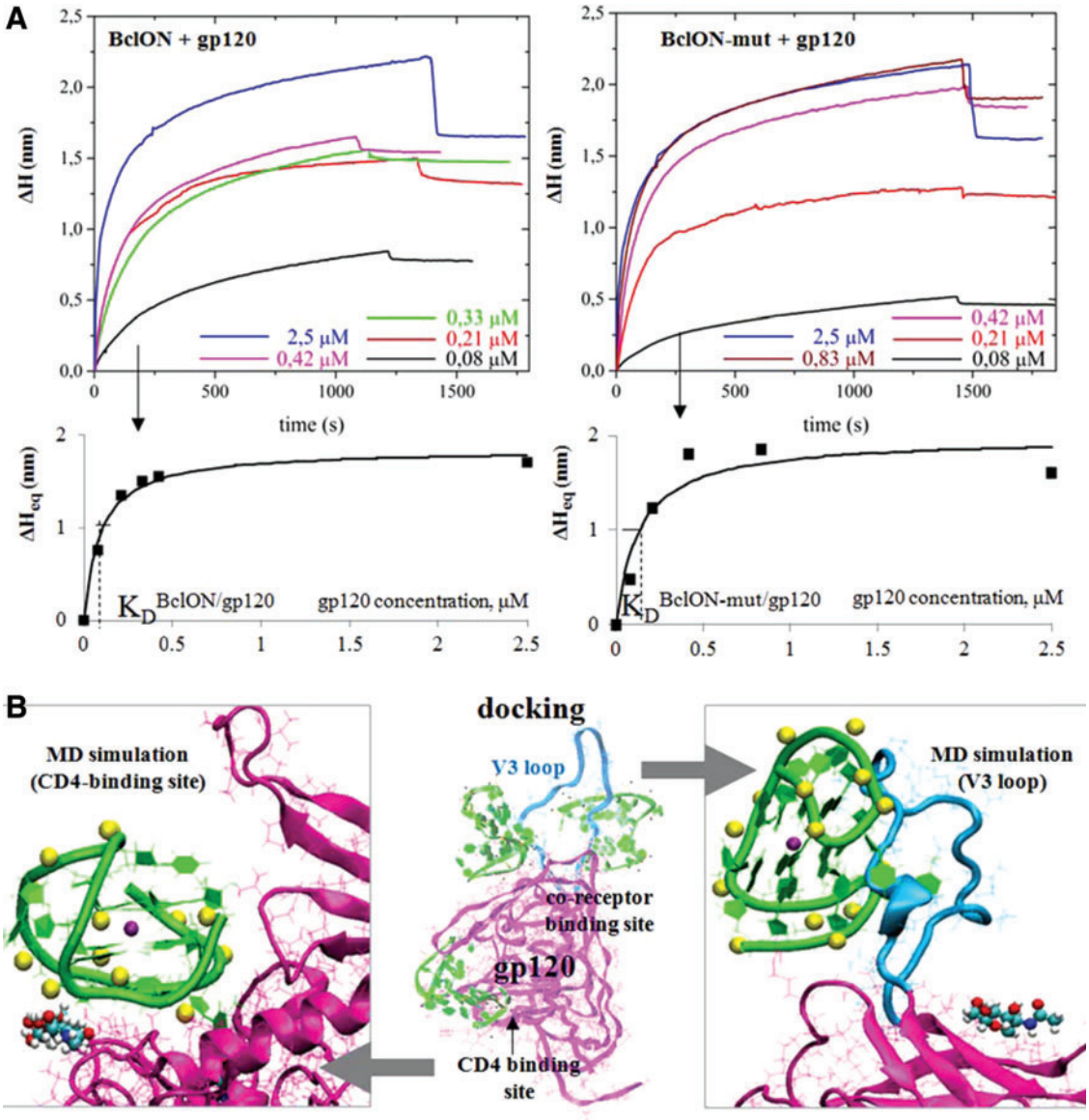

FIG. 2. ON interactions with HIV-1 gp120. **(A)** Assessment of BclON and BclON-mut affinities for gp120 using PCSW biosensors. The sensorgrams (*top graphs*) were obtained upon protein binding with the immobilized ONs. ΔH = increment of the effective adlayer thickness. The solution of gp120 in phosphate-buffered saline (gp120 concentrations are specified in the legends) was run over the aptamer-coated photonic crystal slide surface until the signal reached saturation (~1,000–1,500 s); then, the chamber was washed with the buffer to remove the excess protein (nonspecific binding). The equilibrium ΔH values ($\Delta H_{eq} = \Delta H$ at ~1,600 s) were used to evaluate the Kd of the complexes (*right graphs*). All experiments were performed in duplicate. The standard deviation of ΔH_{eq} did not exceed 10%. **(B)** Molecular modeling of the F-thio-TBA interaction with gp120. The *middle panel* represents the results of (*R/S*)-F-thio-TBA docking to gp120. The *left* and the *right panels* contain MD simulation snapshots for the (*R/S*)-F-thio-TBA complexes with the CD4-bindng site and the V3 loop, respectively. Aptamers, *green*; protein body, *pink*; S atoms, *yellow*; and V3 loop, *blue*. MD, molecular dynamics; PCSW, photonic crystal surface wave; TBA, thrombin-binding aptamer. Color images available online at www.liebertpub.com/nat

protein concentrations (close to the IC_{50}). We synthesized an analog of BclON bearing a fluorescent label (FAM) at the 5′ terminus and a respective quencher (BHQ1) at the 3′ terminus (FAM-BclON-BHQ, m/z calc. $[M+H]^+$, 9050; found, 9052). In the presence of KCl or NaCl, this analog adopts a G4 conformation, FAM and BHQ are drawn together, and the FAM fluorescence is partially quenched. G4 unwinding (ie, upon heating and in the presence of LiCl) results in a ~2-fold increase in the fluorescence intensity (Supplementary Fig. S5A).

We monitored changes in the FAM fluorescence intensity upon the addition of gp120 or pseudo-HIV virions (Supplementary Fig. S5B) in Na^+/K^+-containing working buffers at 20°C (G4 was initially folded under these conditions). The final pseudo-HIV concentration was equal to the concentration used in the activity tests. Fluorescence polarization was also measured in the experiments with gp120.

As expected, the fluorescence polarization significantly increased upon binding (Supplementary Fig. S5B, the right panel). The increase in the fluorescence intensity (both in the experiments with gp120 in PBS and the experiments with pseudo-HIV in the culture media) was relatively small compared with the increase induced by G4 unwinding. The gp120-bound probe would be at least partially shielded from water, so the observed small fluorescence enhancement may be attributed to FAM relocation into a more apolar environment (similar effects have been reported previously for other probes, including fluorescent TBA analogs [73]). Thus, our FRET data indicate that FAM-BclON-BHQ is likely folded in complexes with gp120 and pseudo-HIV. Of course, these results cannot be considered conclusive evidence for the maintenance of G4 in BclON because the label and the quencher may interfere with the binding.

The impact of chemical modifications on aptamer activity

As evident from the IC50 data in Table 1, the thiophosphoryl modification enhanced the anti-HIV activities of the tested ONs. Even partial modification (introduction of thiophosphoryl linkages into TT loops) imparted substantial activity to the initially inactive TBA. Modification throughout the chain was beneficial in both the TBA and BclON series. The addition of a terminal hydrophobic group (DMTr) further increased the F-thio-BclON activity. The effect of the DMTr group was in agreement with previously reported data for Hotoda's G4 ONs that inhibited gp120 binding to CD4 [22].

The positive effect of thio-modification on activity has been observed for a number of anti-HIV aptamers [6,11]. This effect may be due to extra-specific interactions with the target protein. Another possible explanation is that thio-ONs act similarly to dextran sulfate, cyclodextrin sulfate, and heparin (ie, by blocking nonspecific attachment of HIV virions to the cell surface, which precedes the gp120/CD4 interactions) [74].

Thio-modification enhances ON affinities for many proteins due to increased hydrophobicity, and high sequence-independent antiviral activity has been reported for fully modified thiophosphoryl ONs and their 2′-*O*-methylated derivatives [75]. We hypothesized that our thio-aptamers interacted with both viral glycoproteins and cell surface proteins. The latter type of interaction has not been properly analyzed and hopefully will be the subject of future investigations. Here, we report a preliminary estimation of the contribution of the thio modification to specific target recognition based on molecular modeling experiments (docking of the almost inactive TBA and its active F-thio-analog to gp120 and MD simulations for the aptamer/gp120 complexes).

Aptamer docking to gp120 (PDB: 2B4C) was performed to identify the most likely binding sites. Because F-thio-TBA exists as a mixture of a large number of diastereomers (214) with different P configurations, we were unable to model them all; therefore, we only considered three ''boundary'' diastereomers: (*R*)-F-thio-TBA (all P atoms in the *R* configuration), (*S*)-F-thio-TBA (all P atoms in the *S* configuration), and (*R/S*)-F-thio-TBA with alternating *R* and *S* configurations. Figure 2B displays the results of the (*R/S*)-F-thio-TBA docking. For the other diastereomers, see Supplementary Fig. S6. The free energies of aptamer binding with gp120 in the CD4-binding site, the co-receptor-binding site, and the V3 loop estimated using Autodock scoring functions were almost similar (Supplementary Table S1). The aptamers tended to interact with the protein via TT loops.

To further investigate the possible binding modes, we performed MD simulations of the aptamer complexes with the CD4-binding site and the V3 loop. The starting positions and conformations of the aptamers were determined from the docking experiments. In most of the complexes with the co-receptor-binding site, the V3 loop was also involved, so we considered such complexes as well, and the variants with the minimal free energies (Table S1) were selected for MD simulations. The complexes and the G4 cores of TBA and F-thio-TBA were stable throughout the simulation. The representative snapshots for (*R/S*)-F-thio-TBA are shown in Fig. 2B. For other diastereomers, see Supplementary Figs. S7A and S8A. The trajectories are provided as Supplementary Movies.

In the case of the (*S*)-F-thio-TBA complex with the V3 loop, amino acid residues TYR318 and THR320 played major roles in binding. The GLN330 residue from the V3 loop and the ARG440 residue from the nearby region participated in H-bonding with unmodified TBA, (*R*)-F-thio-TBA, and (*R/S*)-F-thio-TBA. In the CD4-binding site, LYS282, LYS487, and ARG480 most significantly contributed to electrostatic interactions and H-bonding with the aptamers. As evident from Fig. 2B and Supplementary Fig. S8A, the disaccharide composed of FUC (alpha-L-fucose) and NDG [2-(acetylamino)-2-deoxy-α-*D*-glucopyranose] residues and attached to the ASN276 residue interacts with all diastereomers of F-thio-TBA.

The estimation of the binding energies by the MM-GBSA method (Supplementary Table S2 and Supplementary Figs. S7B and S8B) revealed that all three analyzed diastereomers of F-thio-TBA were superior to unmodified TBA. Substitution of O for S in the aptamer internucleotide linkages enhanced hydrophobic interactions with the target; the aptamer was drawn into closer proximity and as a result formed more H-bonds with gp120 (Supplementary Figs. S7D and S8D). This result agrees with the data in Tables S1 and S2: the electrostatic binding energy (ΔG_{elec}) is higher in TBA, whereas the van der Waals (ΔG_{vdW}) and total (ΔG_{total}) energies are higher in the thio-aptamers.

To summarize, the molecular modeling results suggest that interactions with gp120 may underlie the observed minor anti-HIV activity of TBA (several gp120 binding sites may be involved, including the V3 loop). The thiophosphoryl TBA

analog has a higher affinity for the gp120V3 loop. Similar to BclON, TBA and its thio analogs appear to retain the G4 conformation upon binding with gp120.

In conclusion, new potent anti-HIV-1 aptamers were obtained. The G4-forming thiophosphoryl ON F-thio-BclON and the unmodified (presumably non-G4-forming at submicromolar concentrations) ON BclON-mut inhibit lentiviral transduction in the low nanomolar range and thus can be considered for the development of microbicides for HIV-1 prevention. Both ONs most likely act via binding with the HIV-1 gp120 glycoprotein, although other targets cannot be excluded.

Acknowledgments

This work was supported by the Russian Science Foundation (14-25-00013) (physicochemical studies, ON synthesis and molecular modeling), the Dynasty Foundation (physicochemical studies—in part), and the Program of Fundamental Research of RAS ''Molecular and Cell Biology'' (activity tests).

Author Disclosure Statement

No competing financial interests exist.

References

1. Sissi C, B Gatto and M Palumbo. (2011). The evolving world of protein-G-quadruplex recognition: a medicinal chemist's perspective. Biochimie 93:1219–1230.
2. Tucker WO, KT Shum and JA Tanner. (2012). G-quadruplex DNA aptamers and their ligands: structure, function and application. Curr Pharm Des 18:2014–2026.
3. Jing N. (2000). Developing G-quartet oligonucleotides as novel anti-HIV agents: focus on anti-HIV drug design. Expert Opin Investig Drugs 9:1777–1785.
4. Musumeci D, C Riccardi and D Montesarchio. (2015). G-quadruplex forming oligonucleotides as anti-HIV agents. Molecules 20:17511–17532.
5. Andreola ML, F Pileur, C Calmels, M Ventura, L Tarrago-Litvak, JJ Toulme and S Litvak. (2001). DNA aptamers selected against the HIV-1 RNase H display in vitro antiviral activity. Biochemistry 40:10087–10094.
6. Wyatt JR, TA Vickers, JL Roberson, RW Buckheit Jr., T Klimkait, E DeBaets, PW Davis, B Rayner, JL Imbach and DJ Ecker. (1994). Combinatorially selected guanosine-quartet structure is a potent inhibitor of human immunodeficiency virus envelope-mediated cell fusion. Proc Natl Acad Sci U S A 91:1356–1360.
7. Koizumi M, R Koga, H Hotoda, T Ohmine, H Furukawa, T Agatsuma, T Nishigaki, K Abe, T Kosaka, *et al.* (1998). Biologically active oligodeoxyribonucleotides. Part 11: the least phosphate-modification of quadruplex-forming hexadeoxyribonucleotide TGGGAG, bearing 3-and 5-end-modification, with anti-HIV-1 activity. Bioorg Med Chem 6:2469–2475.
8. Koizumi M, R Koga, H Hotoda, K Momota, T Ohmine, H Furukawa, T Agatsuma, T Nishigaki, K Abe, *et al.* (1997). Biologically active oligodeoxyribonucleotides—IX. Synthesis and anti-HIV-1 activity of hexadeoxyribonucleotides, TGGGAG, bearing 3′- and 5′-end-modification. Bioorg Med Chem 5:2235–2243.
9. Phan AT, V Kuryavyi, JB Ma, A Faure, ML Andreola and DJ Patel. (2005). An interlocked dimeric parallel-stranded DNA quadruplex: a potent inhibitor of HIV-1 integrase. Proc Natl Acad Sci U S A 102:634–639.
10. Suzuki J, N Miyano-Kurosaki, T Kuwasaki, H Takeuchi, G Kawai and H Takaku. (2002). Inhibition of human immunodeficiency virus type 1 activity in vitro by a new self-stabilized oligonucleotide with guanosine-thymidine quadruplex motifs. J Virol 76:3015–3022.
11. Mazumder A, N Neamati, JO Ojwang, S Sunder, RF Rando and Y Pommier. (1996). Inhibition of the human immunodeficiency virus type 1 integrase by guanosine quartet structures. Biochemistry 35:13762–13771.
12. Jing N, C Marchand, J Liu, R Mitra, ME Hogan and Y Pommier. (2000). Mechanism of inhibition of HIV-1 integrase by G-tetrad-forming oligonucleotides in vitro. J Biol Chem 275:21460–21467.
13. Magbanua E, T Zivkovic, B Hansen, N Beschorner, C Meyer, I Lorenzen, J Grotzinger, J Hauber, AE Torda, *et al.* (2013). d(GGGT) 4 and r(GGGU) 4 are both HIV-1 inhibitors and interleukin-6 receptor aptamers. RNA Biol 10:216–227.
14. Li MH, YH Zhou, Q Luo and ZS Li. (2010). The 3D structures of G-quadruplexes of HIV-1 integrase inhibitors: molecular dynamics simulations in aqueous solution and in the gas phase. J Mol Model 16:645–657.
15. Kelley S, S Boroda, K Musier-Forsyth and BI Kankia. (2011). HIV-integrase aptamer folds into a parallel quadruplex: a thermodynamic study. Biophys Chem 155:82–88.
16. Metifiot M, O Leon, L Tarrago-Litvak, S Litvak and ML Andreola. (2005). Targeting HIV-1 integrase with aptamers selected against the purified RNase H domain of HIV-1 RT. Biochimie 87:911–919.
17. Faure-Perraud A, M Metifiot, S Reigadas, P Recordon-Pinson, V Parissi, M Ventura and ML Andreola. (2011). The guanine-quadruplex aptamer 93del inhibits HIV-1 replication ex vivo by interfering with viral entry, reverse transcription and integration. Antivir Ther 16:383–394.
18. Este JA, C Cabrera, D Schols, P Cherepanov, A Gutierrez, M Witvrouw, C Pannecouque, Z Debyser, RF Rando, *et al.* (1998). Human immunodeficiency virus glycoprotein gp120 as the primary target for the antiviral action of AR177 (Zintevir). Mol Pharmacol 53:340–345.
19. Jing N, E De Clercq, RF Rando, L Pallansch, C Lackman-Smith, S Lee and ME Hogan. (2000). Stability-activity relationships of a family of G-tetrad forming oligonucleotides as potent HIV inhibitors. A basis for anti-HIV drug design. J Biol Chem 275:3421–3430.
20. Hotoda H, M Koizumi, R Koga, M Kaneko, K Momota, T Ohmine, H Furukawa, T Agatsuma, T Nishigaki, *et al.* (1998). Biologically active oligodeoxyribonucleotides. 5. 5′-End-substituted d(TGGGAG) possesses anti-human immunodeficiency virus type 1 activity by forming a G-quadruplex structure. J Med Chem 41:3655–3663.
21. Virgilio A, V Esposito, G Citarella, L Mayol and A Galeone. (2012). Structural investigations on the anti-HIV G-quadruplex-forming oligonucleotide TGGGAG and its analogues: evidence for the presence of an A-tetrad. Chembiochem 13: 2219–2224.
22. Furukawa H, K Momota, T Agatsuma, I Yamamoto, S Kimura and K Shimada. (1997). Identification of a phosphodiester hexanucleotide that inhibits HIV-1 infection in vitro on covalent linkage of its 5′-end with a dimethoxytrityl residue. Antisense Nucleic Acid Drug Dev 7:167–175.
23. Oliviero G, J Amato, N Borbone, S D'Errico, A Galeone, L Mayol, S Haider, O Olubiyi, B Hoorelbeke, J Balzarini and G Piccialli. (2010). Tetra-end-linked oligonucleotides

forming DNA G-quadruplexes: a new class of aptamers showing anti-HIV activity. Chem Commun (Camb) 46: 8971–8973.
24. Di Fabio G, J D'Onofrio, M Chiapparelli, B Hoorelbeke, D Montesarchio, J Balzarini and L De Napoli. (2011). Discovery of novel anti-HIV active G-quadruplex-forming oligonucleotides. Chem Commun (Camb) 47:2363–2365.
25. D'Onofrio J, L Petraccone, E Erra, L Martino, GD Fabio, LD Napoli, C Giancola and D Montesarchio. (2007). 5′-Modified G-quadruplex forming oligonucleotides endowed with anti-HIV activity: synthesis and biophysical properties. Bioconjug Chem 18:1194–1204.
26. Romanucci V, A Marchand, O Mendoza, D D'Alonzo, A Zarrelli, V Gabelica and G Di Fabio. (2016). Kinetic ESI-MS studies of potent anti-HIV aptamers based on the G-quadruplex forming sequence d(TGGGAG). ACS Med Chem Lett 7:256–260.
27. D'Onofrio J, L Petraccone, L Martino, G Di Fabio, A Iadonisi, J Balzarini, C Giancola and D Montesarchio. (2008). Synthesis, biophysical characterization, and anti-HIV activity of glyco-conjugated G-quadruplex-forming oligonucleotides. Bioconjug Chem 19:607–616.
28. Pedersen EB, JT Nielsen, C Nielsen and VV Filichev. (2011). Enhanced anti-HIV-1 activity of G-quadruplexes comprising locked nucleic acids and intercalating nucleic acids. Nucleic Acids Res 39:2470–2481.
29. Marshall WS and MH Caruthers. (1993). Phosphorodithioate DNA as a potential therapeutic drug. Science 259:1564–1570.
30. Oliviero G, J Amato, N Borbone, A Galeone, L Petraccone, M Varra, G Piccialli and L Mayol. (2006). Synthesis and characterization of monomolecular DNA G-quadruplexes formed by tetra-end-linked oligonucleotides. Bioconjug Chem 17:889–898.
31. D'Atri V, G Oliviero, J Amato, N Borbone, S D'Errico, L Mayol, V Piccialli, S Haider, B Hoorelbeke, J Balzarini and G Piccialli. (2012). New anti-HIV aptamers based on tetra-end-linked DNA G-quadruplexes: effect of the base sequence on anti-HIV activity. Chem Commun (Camb) 48: 9516–9518.
32. Sun H and Y Zu. (2015). A highlight of recent advances in aptamer technology and its application. Molecules 20: 11959–11980.
33. Bock LC, LC Griffin, JA Latham, EH Vermaas and JJ Toole. (1992). Selection of single-stranded DNA molecules that bind and inhibit human thrombin. Nature 355:564–566.
34. Zaitseva M, D Kaluzhny, A Shchyolkina, O Borisova, I Smirnov and G Pozmogova. (2010). Conformation and thermostability of oligonucleotide d(GGTTGGTGTGGT TGG) containing thiophosphoryl internucleotide bonds at different positions. Biophys Chem 146:1–6.
35. Kankia BI, G Barany and K Musier-Forsyth. (2005). Unfolding of DNA quadruplexes induced by HIV-1 nucleocapsid protein. Nucleic Acids Res 33:4395–4403.
36. Dapic V, V Abdomerovic, R Marrington, J Peberdy, A Rodger, JO Trent and PJ Bates. (2003). Biophysical and biological properties of quadruplex oligodeoxyribonucleotides. Nucleic Acids Res 31:2097–2107.
37. Scuotto M, E Rivieccio, A Varone, D Corda, M Bucci, V Vellecco, G Cirino, A Virgilio, V Esposito, *et al.* (2015). Site specific replacements of a single loop nucleoside with a dibenzyl linker may switch the activity of TBA from anticoagulant to antiproliferative. Nucleic Acids Res 43: 7702–7716.
38. Martini C, A Hammerer-Lercher, M Zuck, A Jekle, D Debabov, M Anderson and M Nagl. (2012). Antimicrobial and anticoagulant activities of N-chlorotaurine, N,N-dichloro-2,2-dimethyltaurine, and N-monochloro-2,2-dimethyltaurine in human blood. Antimicrob Agents Chemother 56:1979–1984.
39. Lederman MM, RE Offord and O Hartley. (2006). Microbicides and other topical strategies to prevent vaginal transmission of HIV. Nat Rev Immunol 6:371–382.
40. D'Cruz OJ and FM Uckun. (2004). Clinical development of microbicides for the prevention of HIV infection. Curr Pharm Des 10:315–336.
41. Varizhuk AM, VB Tsvetkov, ON Tatarinova, DN Kaluzhny, VL Florentiev, EN Timofeev, AK Shchyolkina, OF Borisova, IP Smirnov, *et al.* (2013). Synthesis, characterization and in vitro activity of thrombin-binding DNA aptamers with triazole internucleotide linkages. Eur J Med Chem 67:90–97.
42. Prokofjeva MM, K Riecken, PV Spirin, DV Yanvarev, A Dusedau, B Ellinger, B Fehse, C Stocking and VS Prassolov. (2013). A new system for parallel drug screening against multiple-resistant HIV mutants based on lentiviral self-inactivating (SIN) vectors and multi-colour analyses. AIDS Res Ther 10:1.
43. Prokofjeva MM, PV Spirin, DV Yanvarev, AV Ivanov, MS Novikov, OA Stepanov, MB Gottikh, SN Kochetkov, B Fehse, C Stocking and VS Prassolov. (2011). Screening of potential HIV-1 inhibitors/replication blockers using secure lentiviral in vitro system. Acta Naturae 3:55–65.
44. Tatarinova O, V Tsvetkov, D Basmanov, N Barinov, I Smirnov, E Timofeev, D Kaluzhny, A Chuvilin, D Klinov, A Varizhuk and G Pozmogova. (2014). Comparison of the 'chemical' and 'structural' approaches to the optimization of the thrombin-binding aptamer. PLoS One 9:e89383.
45. Padmanabhan K and A Tulinsky. (1996). An ambiguous structure of a DNA 15-mer thrombin complex. Acta Crystallogr D Biol Crystallogr 52:272–282.
46. Batista ER, RL Martin and PJ Hay. (2004). Density functional investigations of the properties and thermochemistry of UFn and UCln ($n = 1,\ldots,6$). J Chem Phys 121:11104–11111.
47. Mulliken RS. (1955). Electronic population analysis on LCAO-MO molecular wave functions. J Chem Phys 23:1833–1840.
48. Huang CC, M Tang, MY Zhang, S Majeed, E Montabana, RL Stanfield, DS Dimitrov, B Korber, J Sodroski, *et al.* (2005). Structure of a V3-containing HIV-1 gp120 core. Science 310:1025–1028.
49. Powell MJD. (1977). Restart procedures for the conjugate gradient method. Math Program 12:241–255.
50. Gasteiger G and M Marsili. (1978). A new model for calculating atomic charges in molecules. Tetrahedron Lett 19:3181–3184.
51. Clark M, RD Cramer III and N Van Opdenbosch. (1989). Validation of the general purpose Tripos 5.2 force field. J Comput Chem 10:982–1012.
52. Morris GM, R Huey, W Lindstrom, MF Sanner, RK Belew, DS Goodsell and AJ Olson. (2009). AutoDock4 and AutoDockTools4: automated docking with selective receptor flexibility. J Comput Chem 30:2785–2791.
53. Morris GM, DS Goodsell, RS Halliday, R Huey, WE Hart, RK Belew and AJ Olson. (1998). Automated docking using a Lamarckian genetic algorithm and an empirical binding free energy function. J Comput Chem 19:1639–1662.

54. Mehler EL and T Solmajer. (1991). Electrostatic effects in proteins: comparison of dielectric and charge models. Protein Eng 4:903–910.
55. Stouten PFW, C Frömmel, H Nakamura and C Sander. (1993). An effective solvation term based on atomic occupancies for use in protein simulations. Mol Simul 10: 97–120.
56. Ryckaert J-P, G Ciccotti and HJC Berendsen. (1977). Numerical integration of the cartesian equations of motion of a system with constraints: molecular dynamics of n-alkanes. J Comput Phys 23:327–341.
57. Pozmogova GE, MA Zaitseva, IP Smirnov, AG Shvachko, MA Murina and VI Sergeenko. (2010). Anticoagulant effects of thioanalogs of thrombin-binding DNA-aptamer and their stability in the plasma. Bull Exp Biol Med 150: 180–184.
58. Stein CA. (1996). Exploiting the potential of antisense: beyond phosphorothioate oligodeoxynucleotides. Chem Biol 3:319–323.
59. Shahid R, A Bugaut and S Balasubramanian. (2010). The BCL-2 5′ untranslated region contains an RNA G-quadruplex-forming motif that modulates protein expression. Biochemistry 49:8300–8306.
60. Xiao J, JA Carter, KA Frederick and LB McGown. (2009). A genome-inspired DNA ligand for the affinity capture of insulin and insulin-like growth factor-2. J Sep Sci 32:1654–1664.
61. Membrino A, S Cogoi, EB Pedersen and LE Xodo. (2011). G4-DNA formation in the HRAS promoter and rational design of decoy oligonucleotides for cancer therapy. PLoS One 6:e24421.
62. Miglietta G, AS Gouda, S Cogoi, EB Pedersen and LE Xodo. (2015). Nucleic acid targeted therapy: G4 oligonucleotides downregulate HRAS in bladder cancer cells through a decoy mechanism. ACS Med Chem Lett 6:1179–1183.
63. Yoshida W, T Saito, T Yokoyama, S Ferri and K Ikebukuro. (2013). Aptamer selection based on G4-forming promoter region. PLoS One 8:e65497.
64. Chang T, C Qi, J Meng, N Zhang, T Bing, X Yang, Z Cao and D Shangguan. (2013). General cell-binding activity of intramolecular G-quadruplexes with parallel structure. PLoS One 8:e62348.
65. Bates PJ, DA Laber, DM Miller, SD Thomas and JO Trent. (2009). Discovery and development of the G-rich oligonucleotide AS1411 as a novel treatment for cancer. Exp Mol Pathol 86:151–164.
66. Gray DM, JD Wen, CW Gray, R Repges, C Repges, G Raabe and J Fleischhauer. (2008). Measured and calculated CD spectra of G-quartets stacked with the same or opposite polarities. Chirality 20:431–440.
67. Li XM, KW Zheng, JY Zhang, HH Liu, YD He, BF Yuan, YH Hao and Z Tan. (2015). Guanine-vacancy-bearing G-quadruplexes responsive to guanine derivatives. Proc Natl Acad Sci U S A 112:14581–14586.
68. Mukundan VT and AT Phan. (2013). Bulges in G-quadruplexes: broadening the definition of G-quadruplex-forming sequences. J Am Chem Soc 135:5017–5028.
69. Prinz H. (2010). Hill coefficients, dose-response curves and allosteric mechanisms. J Chem Biol 3:37–44.
70. Wilen CB, JC Tilton and RW Doms. (2012). HIV: cell binding and entry. Cold Spring Harb Perspect Med 2: a006866.
71. Juliano RL and K Carver. (2015). Cellular uptake and intracellular trafficking of oligonucleotides. Adv Drug Deliv Rev 87:35–45.
72. Konopsky VN and EV Alieva. (2009). Optical biosensors based on photonic crystal surface waves. Methods Mol Biol 503:49–64.
73. De Tito S, F Morvan, A Meyer, JJ Vasseur, A Cummaro, L Petraccone, B Pagano, E Novellino, A Randazzo, C Giancola and D Montesarchio. (2013). Fluorescence enhancement upon G-quadruplex folding: synthesis, structure, and biophysical characterization of a dansyl/cyclodextrin-tagged thrombin binding aptamer. Bioconjug Chem 24: 1917–1927.
74. Callahan LN, M Phelan, M Mallinson and MA Norcross. (1991). Dextran sulfate blocks antibody binding to the principal neutralizing domain of human immunodeficiency virus type 1 without interfering with gp120-CD4 interactions. J Virol 65:1543–1550.
75. Vaillant A, JM Juteau, H Lu, S Liu, C Lackman-Smith, R Ptak and S Jiang. (2006). Phosphorothioate oligonucleotides inhibit human immunodeficiency virus type 1 fusion by blocking gp41 core formation. Antimicrob Agents Chemother 50:1393–1401.

Address correspondence to:
Galina Pozmogova, ScD
Federal Research and Clinical Center of Physical-Chemical Medicine of Federal Medical Biological Agency
Malaya Pirogovskaya 1a
Moscow 119435
Russia

E-mail: pozmogova@niifhm.ru

Anna Varizhuk, PhD
Federal Research and Clinical Center of Physical-Chemical Medicine of Federal Medical Biological Agency
Malaya Pirogovskaya 1a
Moscow 119435
Russia

E-mail: annavarizhuk@niifhm.ru

Sergey N. Mikhailov, ScD
Engelhardt Institute of Molecular Biology RAS
Moscow 119991
Russia

E-mail: smikh@eimb.ru

Received for publication April 22, 2016; accepted after revision September 25, 2016.